Supporting Information

Burgos et al. 10.1073/pnas.0903898106

SI Text

Protein Expression and Purification. The enzyme was overexpressed in *Escherichia coli* BL21(DE3)p*Lys* containing the expression plasmid pBAD DEST 49 with inserts of chemically synthesized DNA (DNA 2.0) encoding for human NAMPT and optimized for expression in *E. coli*. The soluble protein was purified by Ni-NTA affinity chromatography, and gel-filtration (HiLoad Superdex 200GP 26/60). The human NAMPT (10 mg mL^{-1}) was concentrated to 50–75 mg mL^{-1} in a buffer containing 20 mM Tris pH 7.5, 100 mM NaCl, and 10 mM βME and stored at -80 °C.

ADP/ATP Isotope Exchange Assay. ADP/ATP isotope exchange reactions were carried out in 50 mM Hepes pH 7.5 with 50 mM NaCl, 5 mM free $MgCl_2$, and 1 mM THP at 25 °C. ADP (200 μM, containing 10^5 cpm of [2, 8-^{3}H]ADP per 100 μM cold ADP) and ATP (1 mM) were present as equimolar mixtures with $MgCl_2$. The reactions were started by addition of 0.6 μM enzyme and 4 samples were quenched at 15-min intervals. Nucleotides were separated by HPLC to determinate the rate of the exchange reaction. The effect of BeF_3^- on the exchange rate was monitored by incubating NAMPT (0.6 μM) with 6.2 mM $MgCl_2$, 20 mM NaF, and varying concentrations of $BeCl_2$ (0 to 500 μM) during 2 periods of time (15 and 60 min, respectively); followed by the addition of a small volume to make the final concentrations of ADP 200 μM, containing 10^5 cpm of [2, 8-^{3}H]ADP per 100 μM cold ADP, then ATP (1 mM) was rapidly added to initiate the exchange reaction. Determination of the exchange rates was performed as above.

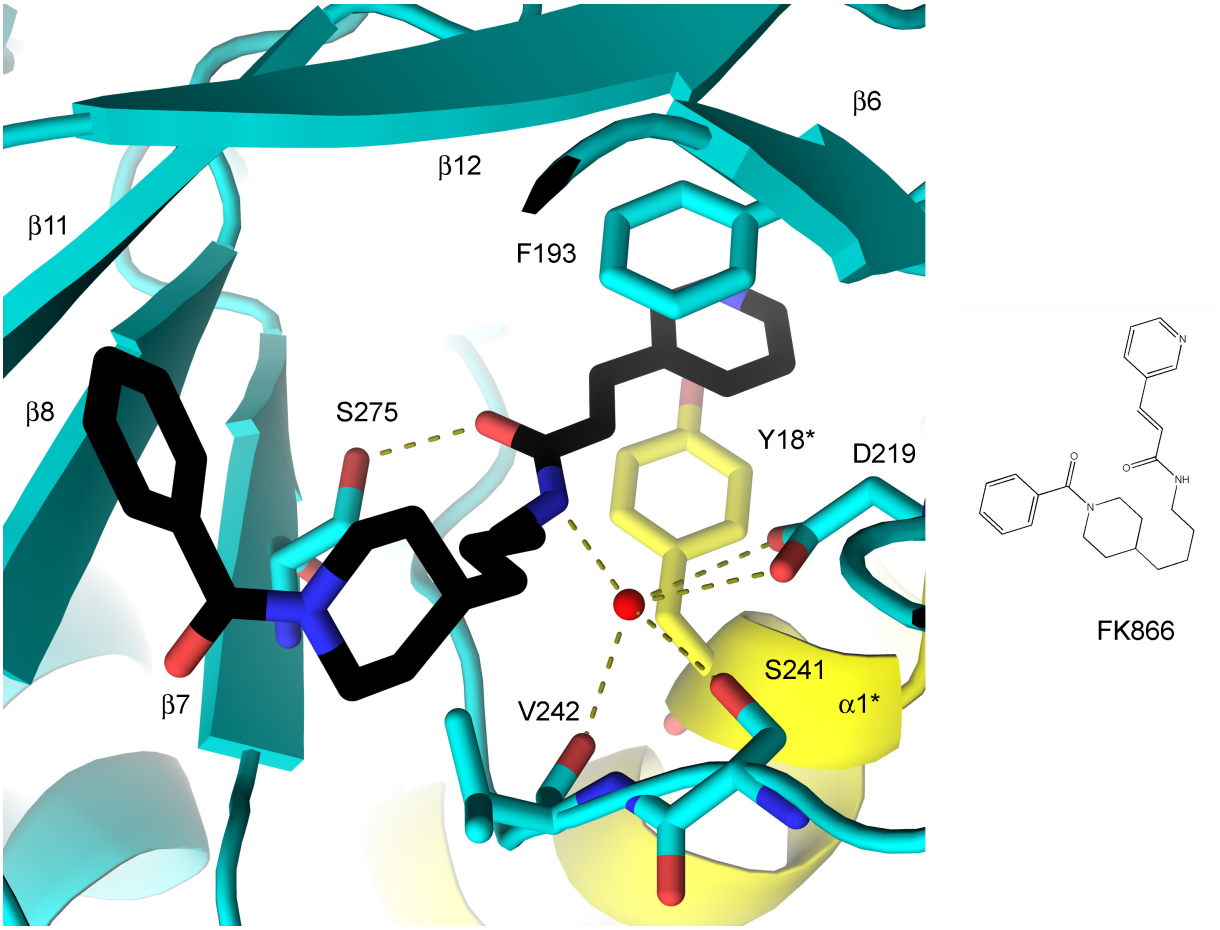

Fig. S1. Human NAMPT bound to FK866. Structure with 1 monomer in yellow, the other one in cyan. FK866 is depicted in black while water molecule is depicted as red sphere and olive dash lines represent hydrogen bonds between the inhibitor and residues of both monomers (PDB accession code 2GVJ). Produced with Pymol v 1.1.

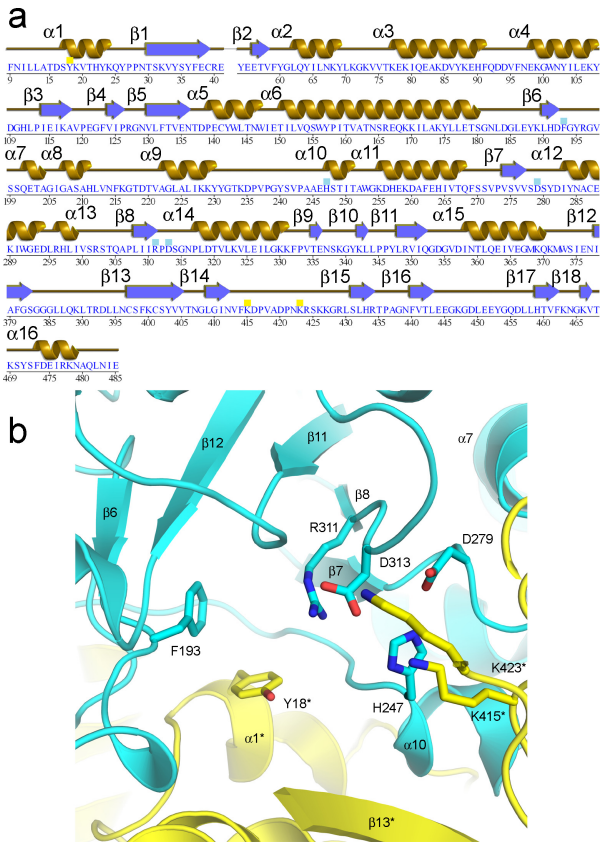

Fig. S2. Structure of Human NAMPT. (*a*) Structure-based sequence of human NAMPT. α-Helices and β-strands are indicated above the sequence. Cyan and yellow squares are residues from the active site (involved in π-stacking interaction with the aromatic moiety of benzamide, NMN, and/or AMPcP; involved in hydrogen bonds with the diphosphate moiety of substrates and products or also the triad of residues conserved in all NAMPT and NAPT enzymes, including H247 at the proposed autophosphorylation site). (*b*) Ribbon diagram showing a close-up of the active site region. Elements and residues with * are part of the monomer 1 (colored in yellow), others are from the monomer 2 (colored in cyan; AMPcP has been removed to simplify the figure). Produced with PyMol v 1.1.

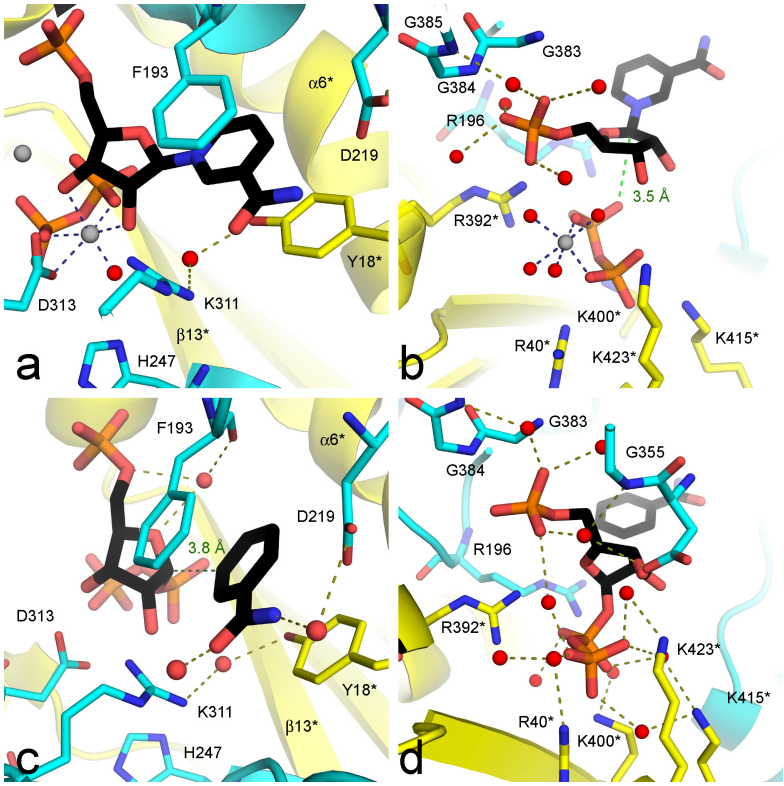

Fig. S3. Active site of H247-unmodified human NAMPT in interaction with the bimolecular complex NMN·Mg_2PPi and PRPP·BzAM. The 2 monomers are colored in yellow and cyan, blue dash lines represent Mg^{2+} (as gray spheres) interactions with PPi moiety. Water molecules are represented as red spheres and the corresponding hydrogen bonds shown as olive dash lines. (*a*) Presentation of the main interactions for the NAM and ribose moieties. NMN is shown in black. (*b*) Presentation of the main interactions for the diphosphate moiety. Green dash line represents interatomic distance d_2 as summarized in Table 1. (*c*) Main interactions for the BzAM and ribose moieties (black). Green dash line represents interatomic distance d_1 as summarized in Table 1. (*d*) Presentation of the main interactions for the diphosphate moiety. Produced with PyMol v 1.1.

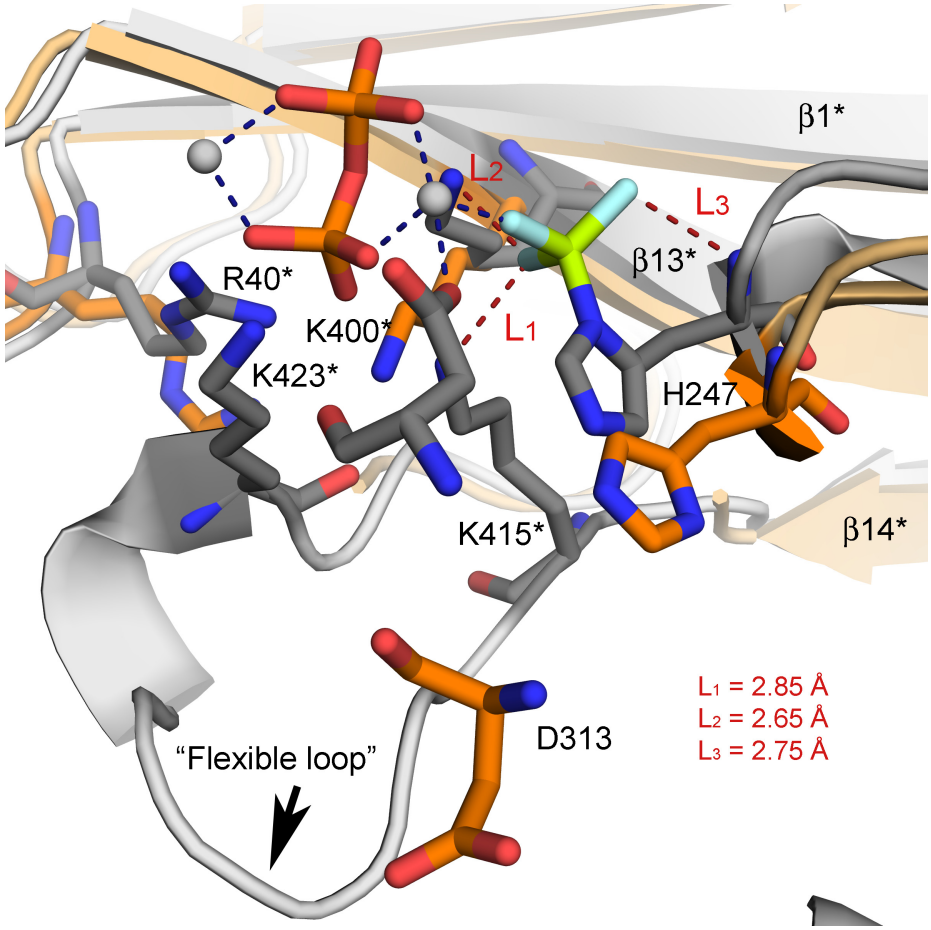

Fig. S4. The loop linking β14* to β15* and its induced motion upon PPi binding and phosphorylation of H247. Orange ribbons and residues represent the apo form of *Rattus norvegicus* NAMPT (2G95) while the second layer (gray) represents the (Nδ1)H247-BeF_3^-·NMN·Mg_2PPi complex of human NAMPT (3DHF). Blue dash lines represent Mg^{2+} (gray spheres) interactions with PPi and BeF_3^-; red dash lines represent interatomic distances L_1, L_2, and L_3. Produced with PyMol v 1.1.

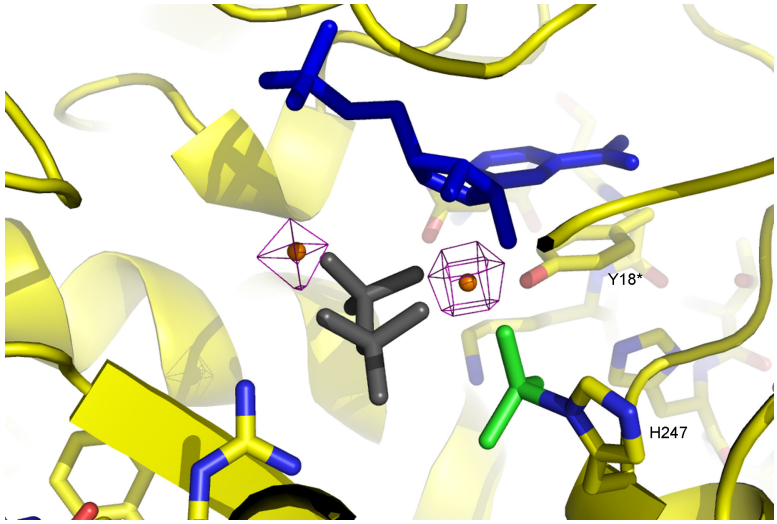

Fig. S5. The Mn^{2+} anomalous difference Fourier map at 10σ level. The 2 peaks from Mn^{2+} anomalous difference Fourier map (colored in magenta) are overlaid perfectly with the 2 magnesium ions. The NMN, PPi, and BeF_3^- are colored in blue, gray, and green, respectively. Produced with PyMol v 1.1.

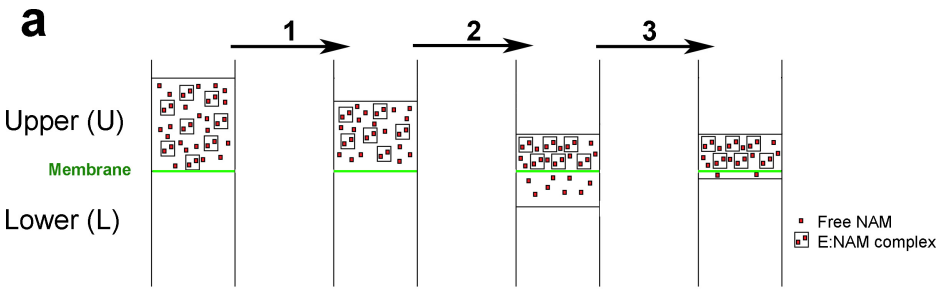

1: 25 μL of homogeneous solution collected (cpm U)
2: sample spining down
3: 25 μL of homogeneous solution collected (cpm L)

b

$$A = [NAM]^{free} = [NAM]^{L} = [NAM]^{oU}\frac{cpm^{L}}{cpm^{oU}}$$

$$r = \frac{[E:NAM]}{[E]^{o}} = \frac{[NAM]^{oU}}{[E]^{o}}\left(1 - \frac{cpm^{L}}{cpm^{oU}}\right) \qquad \text{(with R, binding stoichiometry)}$$

$$\frac{1}{r} = \frac{1}{R} + \frac{K_d}{R}\frac{1}{A}$$

c

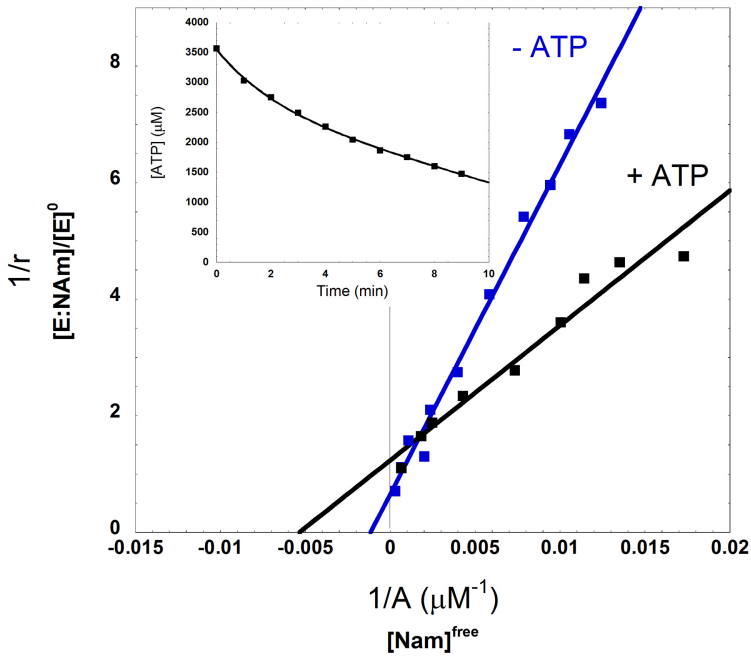

Fig. S6. Determination of the dissociation constants (K_d) by ultrafiltration for NAM with phosphorylated and nonphosphorylated human NAMPT. (*a*) Details of the method used for the assay. (*b*) Equations and relations between the concentration of free substrate (*A*), the bound- vs. free-enzyme ratio (*r*) and the stoichiometry of binding (*R*). (*c*) Graphic representation of the corresponding results; the insert confirms that even after the 10 min required for the determination, ATP is still hydrolyzed and the enzyme remains phosphorylated.

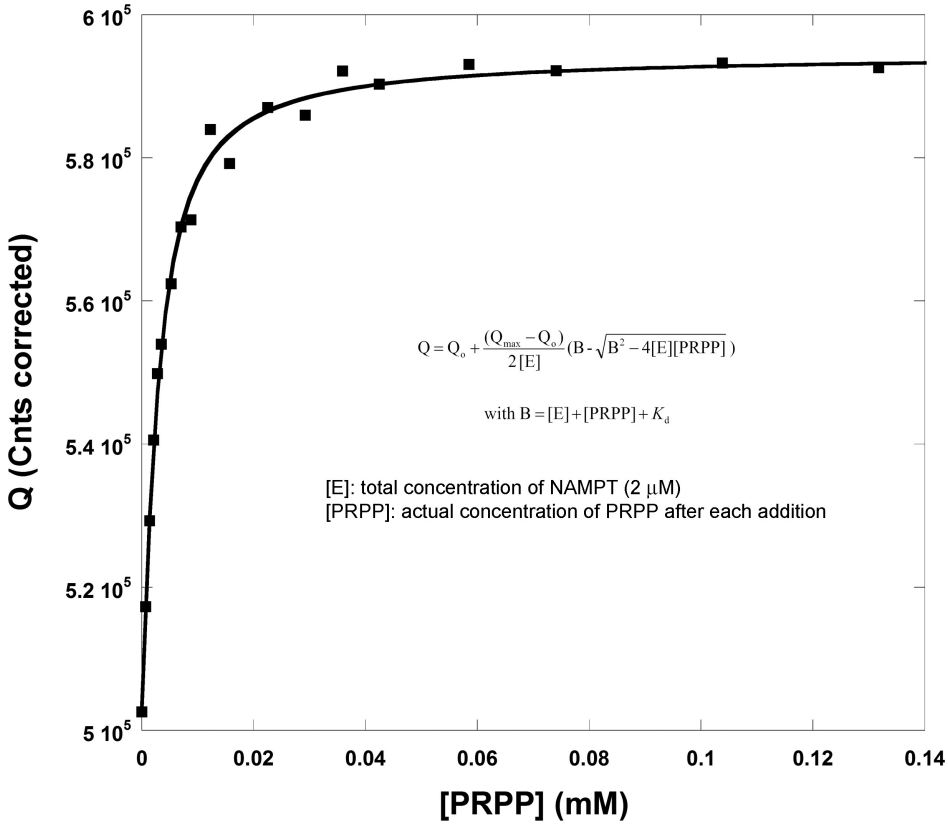

Fig. S7. Determination of the dissociation constant (K_d) for PRPP by fluorescence with phosphorylated human NAMPT. The typical equation (solution for the second order polynomial expression of K_d) fits the variations of fluorescence observed upon addition of PRPP on the phosphorylated enzyme.

Table S1. Data collection and refinement statistics

	AMPcP	NMN and PPi	NMN and PPi (BeF_3^- form)	PRPP and BzAM	PRPP and BzAM (BeF_3^- form)
PDB codes	3DGR	3DHD	3DHF	3DKJ	3DKL
Data collection					
Space group	$P2_1$	$P2_1$	$P2_1$	$P2_1$	$P2_1$
Cell dimension					
a, b, c (Å)	61.3, 107.2, 82.7	61.2, 107.1, 83.3	61.0, 106.4, 83.4	61.2, 107.1, 83.3	61.2, 107.1, 83.3
α, β, γ (°)	90, 96.4, 90	90, 97, 90	90, 96.9, 90	90, 97, 90	90, 97, 90
Resolutions (Å)	20–2.1 (2.17–2.10)	20–2.0 (2.07–2.0)	50–1.8 (1.86–1.80)	20–2.0 (2.07–2.0)	50–1.9 (1.97–1.89)
R_{merge} (%)	7.4 (24.7)	6.8 (20.4)	5.4 (27.3)	6.1 (21.6)	8.2 (35.8)
$I / \sigma I$	8.3 (2.4)	18.3 (4.5)	8.2 (2.6)	22.1 (3.8)	7.1 (2.2)
Completeness (%)	94.5 (63.6)	96.7 (75.2)	99.6 (96.5)	95.9 (73.9)	97.2 (82.0)
Redundancy	3.6 (2.5)	3.6 (2.9)	4.1 (3.3)	3.9 (2.8)	3.9 (2.7)
Refinement					
Resolution (Å)	20–2.1	20–2.0	25.9–1.8	19.9–2.0	28.6–1.9
No. reflections	58,607	69,501	97,445	68,540	81,743
R_{work} / R_{free} (%)	18.0 / 22.5	18.0 / 22.1	16.0 / 19.6	16.8 / 20.9	17.7 / 21.4
B-factors (Å^2)					
Protein					
(main chain)	32.5	23.4	22.6	23.4	16.5
(side chain)	34.7	25.1	24.7	25.1	19.1
Water	34.1	27.3	26.6	27.3	25.4
Ligand	42.4	24.6	13.9	31.1	20
NMN or PRPP		23.1	13.5	35.7	20
PPi or BzAM		26.8	14.1	19.8	18.7
BeF_3^-			14.2		21.2
R.m.s deviations					
Bond lengths (Å)	0.016	0.018	0.014	0.014	0.019
Bond angles (°)	1.49	1.60	1.45	1.50	1.69

Numbers in parentheses are for the highest-resolution shell. One crystal was used for each data set.